Flight Control Law Design using Hybrid Incremental Nonlinear Dynamic Inversion

Kumtepe, Y.; Pollack, T.S.C.; van Kampen, E.

DOI
10.2514/6.2022-1597

Publication date
2022

Document Version
Final published version

Published in
AIAA SCITECH 2022 Forum

AIAA SciTech Forum
January 3-7, 2022, San Diego, CA & Virtual
AIAA SCITECH 2022 Forum

10.2514/6.2022-1597

Flight Control Law Design Using Hybrid Incremental Nonlinear Dynamic Inversion

Y. Kumtepe*
Roketsan Inc., 06780, Ankara, Turkey

T.S.C. Pollack†, and E. van Kampen‡
Delft University of Technology, 2629HS Delft, The Netherlands

Incremental Nonlinear Dynamic Inversion (INDI) is a sensor-based control strategy, which has shown robustness against model uncertainties on various aerospace platforms. The sensor-based nature of the method brings attractive properties, which has made it popular in the last decade. INDI globally linearizes the system by making use of control input and state derivative feedback. Despite the enhanced robustness against parametric system uncertainties compared to traditional NDI, mitigating the effects of time lag between the control input and state derivative feedback paths represents an important challenge for INDI. Past research has shown that this can be addressed by synchronizing these feedback signals, although the method remains vulnerable to unexpected measurement delays. This paper proposes a hybrid INDI approach based on complementary filtering to further mitigate this robustness issue. The approach fuses the system model and sensor measurement to generate an estimate of the angular acceleration of the system. The estimation responds rapidly to the system input thanks to the on-board model, whereas adequate accuracy in the low-to-medium frequency range is maintained by the sensor measurement. The control law is found to retain good performance in case of model mismatches and measurement delays. To demonstrate the method, a hybrid INDI-based attitude control law is designed for a nonlinear F-16 aircraft model. The robustness properties of the resulting control system are analyzed using time-domain simulations.

Nomenclature

b, $\bar{c}$, S	=	Wing span, mean aerodynamic chord, surface area
C_l, C_m, C_n	=	Aerodynamic moment coefficients
h	=	Altitude
J	=	Inertia matrix, cost function
$\boldsymbol{K}$	=	Control gains matrix
L, M, N	=	Aircraft moments
$\boldsymbol{u}$	=	Input vector
V	=	Velocity
$\boldsymbol{y}$	=	Output vector
$\boldsymbol{x}$	=	State vector
α, β	=	Angle of attack, side slip angle
δ	=	Control surface deflection
ϵ	=	Root mean square of tracking error
ζ	=	Damping coefficient
$\boldsymbol{\theta}$	=	Attitude angles
ρ	=	Air density
ϕ, θ, ψ	=	Roll angle, pitch angle, yaw angle
p, q, r	=	roll rate, pitch rate and yaw rate
$\boldsymbol{\omega}$	=	Angular rate vector
ω_n	=	Natural frequency

*Engineer, Advanced Technologies and Systems, Roketsan, Inc., 06780, Ankara, Turkey
†Ph.D. Student, Control and Simulation Division, Faculty of Aerospace Engineering, Kluyverweg 1, 2629HS Delft, the Netherlands
‡Assistant Professor, Control and Simulation Division, Faculty of Aerospace Engineering, Kluyverweg 1, 2629HS Delft, the Netherlands

Subscripts

d	=	desired
e, r, a, th	=	elevator, rudder, aileron, thrust
m, s, r	=	model, sensor and reference
sync	=	synchronization

I. Introduction

Adequate stability and flying quality characteristics represent key flight control law design objectives and are vital for overall aircraft safety and performance levels. However, the nature of gain-scheduled control laws based on classical control design methods do not provide stability and guarantee performance between design points. In this view, Nonlinear Dynamic Inversion (NDI) has been proposed as a useful alternative to the practice of gain scheduling [1, 2]. This control strategy has appealing properties such as global linearization of input-output dynamics, decoupling control channels, and being readily transferable among different types of vehicles while requiring only minor modifications. However, NDI requires an accurate model representation of the complete system, which may not be straightforward to obtain. Pilot workload may increase considerably in case of uncompensated uncertainties and system failures, whereas stability margins may be compromised as well. This problem has been addressed in various ways in the past, such as through the use of robust control methods or by incorporating adaptive schemes based on real-time system identification [3].

In order to mitigate the drawbacks of NDI without compromising on its appealing properties, Incremental Nonlinear Dynamic Inversion (INDI) has been proposed as a solution [4, 5]. INDI depends only on a model of the control effectiveness part of the plant dynamics, which makes it inherently more robust to parametric system uncertainties compared to traditional NDI. The main advantage of the method lies in the measurement of system acceleration, which contains direct information about the system dynamics such as nonlinearities and gust-induced disturbances. Having direct access to this information is especially useful when plant modeling is challenging or expensive. The beneficial properties of INDI have been demonstrated on various platforms and applications, such as the Cessna Citation II flying research aircraft [6–8], quadrotor UAVs [9], and a hybrid tailsitter UAV [10]. The nature of the method also implies inherent robustness against a wide range of faults and structural damages. The tolerance of INDI against actuator faults has been shown in various studies, which indicates the ability of the method to extend the flight envelope in failure conditions [11–13].

Despite its enhanced robustness against parametric system uncertainties, the performance of INDI tends to be impaired by measurement delays. Studies on helicopter and spacecraft dynamics have shown the method's success on tracking performance and rejecting disturbances, but also demonstrated the method's limitations based on sampling frequency and measurement delays [14, 15]. This can be considered as a direct consequence of the increased sensor measurement dependency of INDI. Sensors transmit information about model mismatches and disturbances but due to limited sampling frequencies, noise filtering, and other processes, the obtained measurement may not correspond to the true system value at the correct instant in time. In fact, this is considered as one of the main challenges of INDI [6, 16]. The use of angular accelerometers instead of gyroscopes may lead to improvements in this regard, although they are not very common in the aerospace domain [7, 17]. Nevertheless, past studies have shown that satisfactory performance can be achieved when actuator measurements are matched in time by using synchronization filters [6, 9, 16].

In this paper, a Hybrid INDI strategy based on complementary filtering is proposed that features enhanced robustness against measurement delays. The main contributions of the paper are as follows. First, the Hybrid INDI approach is presented. The complementary filtering strategy fuses model outputs with sensor measurements, keeping the beneficial characteristics of both signals. Second, an analysis of Hybrid INDI-based control laws is presented focusing on the synchronization method and performance when there are measurement delays. This analysis includes closed-loop pole migrations of the system and time-domain simulation comparisons of Hybrid INDI and Sensor-Based INDI. Lastly, a Hybrid INDI-based flight control law is designed for an F-16 aircraft model, and the robustness of different INDI approaches against sensor delays and aerodynamic uncertainties is investigated

The paper briefly discusses the fundamental theory and formulations of INDI in Section II. Section III introduces Hybrid INDI as well as the complementary filter used for the angular acceleration estimation, and shows improvements in robustness of Hybrid INDI compared to Sensor-Based INDI. Section IV explains the application of Hybrid INDI in the context of an attitude control law design. Various simulation results are presented and the INDI approaches are compared in terms of nominal performance, disturbance rejection, and handling measurement delays in Section V. Lastly, the article is concluded in Section VI.

II. Incremental Nonlinear Dynamic Inversion

INDI is inspired by NDI, which is based on feedback linearization principles. The main principle of NDI is to linearize the input-output relation of a nonlinear input-affine system by using state feedback and coordinate transformation rather than Jacobian linearization. Consequently, the dynamics of the controlled variables are reduced to simple integrator dynamics. As a result, the system can be controlled using linear control methods. Fundamentally, the method requires a model of the system that is fully accurate. However, real systems are generally highly complex and obtaining their accurate model may be difficult. INDI is proposed to reduce model dependency to the control effectiveness matrix [18]. This section introduces the key concepts of INDI. Two versions of INDI are presented, (i) Sensor-Based INDI that is referred to as the conventional INDI method in the literature, and (ii) Model-Based INDI, which is an incremental method that uses the system model.

A. Sensor-Based INDI

A general nonlinear control-affine system has the form of

$$\dot{\boldsymbol{x}} = \boldsymbol{f}(\boldsymbol{x}) + \boldsymbol{g}(\boldsymbol{x})\boldsymbol{u}. \tag{1}$$

$$\boldsymbol{y} = \boldsymbol{h}(\boldsymbol{x}) \tag{2}$$

where $\boldsymbol{x} \in \mathbb{R}^n$ represents the state vector , $\boldsymbol{u} \in \mathbb{R}^m$ the input vector, $\boldsymbol{y} \in \mathbb{R}^p$ the output vector, $\boldsymbol{f}$ and $\boldsymbol{h}$ are smooth vector fields, and $\boldsymbol{g} \in R^{n\times m}$ is a matrix with smooth vector field columns that represents the state-dependent control matrix. This equation can be approximated by taking the Taylor series expansion at the current value of the state $\boldsymbol{x}_0$ and control input $\boldsymbol{u}_0$ as

$$\dot{\boldsymbol{x}} \approx \boldsymbol{f}(\boldsymbol{x}_0) + \boldsymbol{g}(\boldsymbol{x}_0)\boldsymbol{u}_0 + \frac{\partial}{\partial \boldsymbol{x}}\left[\boldsymbol{f}(\boldsymbol{x}) + \boldsymbol{g}(\boldsymbol{x})\boldsymbol{u}\right]_{\boldsymbol{u}_0,\boldsymbol{x}_0}(\boldsymbol{x} - \boldsymbol{x}_0) + \frac{\partial}{\partial \boldsymbol{u}}\left[\boldsymbol{f}(\boldsymbol{x}) + \boldsymbol{g}(\boldsymbol{x})\boldsymbol{u}\right]_{\boldsymbol{u}_0,\boldsymbol{x}_0}(\boldsymbol{u} - \boldsymbol{u}_0). \tag{3}$$

Higher order terms are assumed to be negligible and are therefore not included in the expression. The summation of first two terms is simply $\dot{\boldsymbol{x}}_0$. Generally, in aerospace applications controls change much faster than the states. This leads to assumption of $\boldsymbol{x} = \boldsymbol{x}_0$, meaning that the change of the state between two time steps is negligible as a result of time scale separation between states and inputs. The validity of time scale separation is one of the main assumptions in the INDI derivation. The increment in control input is defined as $\Delta\boldsymbol{u} = \boldsymbol{u} - \boldsymbol{u}_0$. Then, Eq. (3) reduces to

$$\dot{\boldsymbol{x}} \approx \dot{\boldsymbol{x}}_0 + \boldsymbol{g}(\boldsymbol{x}_0)\Delta\boldsymbol{u}. \tag{4}$$

The incremental control law is formed based on the relation in Eq. (4). For this system, it is assumed that the state variables are also the outputs, *i.e.* $\dot{\boldsymbol{x}} = \dot{\boldsymbol{y}}$. A virtual control input is the input to the linearization loop and it is defined as $\boldsymbol{\nu} = \dot{\boldsymbol{x}}$. The virtual control vector is designed by linear controllers based on the characteristics of the desired dynamics of the control variables. This will be further elaborated on in Section IV. Subsequently, the control increment is determined as

$$\Delta\boldsymbol{u} = \boldsymbol{g}^{-1}(\boldsymbol{x}_0)(\boldsymbol{\nu} - \dot{\boldsymbol{x}}_0). \tag{5}$$

The new control input is given based on the previous control input, control effectiveness matrix and virtual control input as

$$\boldsymbol{u} = \boldsymbol{u}_0 + \boldsymbol{g}^{-1}(\boldsymbol{x}_0)(\boldsymbol{\nu} - \dot{\boldsymbol{x}}_0). \tag{6}$$

It is evident from this result that the obtained control law is not dependent on the plant dynamics term $\boldsymbol{f}(\boldsymbol{x})$. The dependency of control law on an available model reduces to the control effectiveness matrix only, at the expense of requiring access to $\dot{\boldsymbol{x}}_0$ and $\boldsymbol{u}_0$. Sensor-Based INDI obtains the value of $\dot{\boldsymbol{x}}_0$ based on sensor measurements. These measurements are generally not perfect and may be corrupted by time lag, bias and noise in real life applications. In fact, it may not even be possible to measure the state derivative $\dot{\boldsymbol{x}}$ directly.

In Sensor-Based INDI control laws, the control input depends on the most recent state derivative, $\dot{\boldsymbol{x}}_0$. Sensors measure this value, and the signal is filtered to alleviate the noise. The sensor dynamics cause $\dot{\boldsymbol{x}}_0$ not to be available for the use of controller until future time. The available state derivative value is denoted as $\dot{\boldsymbol{x}}_f$ because it is the output of the noise filter. Using this value directly without taking any other measures causes degradation in performance and typically leads to oscillatory control system responses. Studies show that the oscillatory motion of INDI-based control systems can be prevented by changing the modeled control effectiveness matrix by a factor [19, 20]. Increasing control effectiveness reduces control input since the control law reverses $\boldsymbol{g}$. It eventually makes the system less aggressive and

less agile. A more common and theoretically proven method is the synchronization of the input signal with the expected measurement delay [9].

Assuming accurate knowledge of the actuator position means that the most recent value $\boldsymbol{u}_0$ is available and previous values are also achievable. In order to match the control input to the measurement, the input is filtered by the sensor and noise filter dynamics. In this way, $\boldsymbol{u}_f$ is obtained and the Sensor-Based INDI control law from Eq. 6 is rewritten as

$$\boldsymbol{u} = \boldsymbol{u}_f + \boldsymbol{g}^{-1}(\boldsymbol{x}_f)(\boldsymbol{\nu} - \dot{\boldsymbol{x}}_f). \tag{7}$$

Ensuring synchronous signals is regarded as the key for practical implementations of INDI [6]. As the state derivative matches with control input in time, dynamics that cause performance deterioration are eliminated [9]. These dynamics reappear when there is an unexpected additional lag in the signals. As the time mismatch between the signals increases, the tracking error also increases [16].

Several assumptions have been made in the derivation of the control law, such as neglecting higher order terms and assuming negligible state increment contributions. The validity of the assumptions are studied in [14, 15]. The results show that sampling time is one of the factors that might reduce the performance. Using a low-sampling-rate flight computer causes the change in states to be non-negligible. There are different studies which derive INDI control without using time scale separation and show the stability of the method with less assumptions [21].

B. Model-Based INDI

Model-Based INDI is formulated based on the same procedure of Sensor-Based INDI. The Taylor series expansion given in Eq. (3) replaces the true dynamics, $\boldsymbol{f}(\boldsymbol{x}_0) + \boldsymbol{g}(\boldsymbol{x}_0)\boldsymbol{u}_0$, with $\dot{\boldsymbol{x}}_0$. For the derivation of Model-Based INDI, modeled dynamics, $\boldsymbol{f}_{\text{mod}}(\boldsymbol{x}_0) + \boldsymbol{g}_{\text{mod}}(\boldsymbol{x}_0)\boldsymbol{u}_0$, replace the true dynamics, and the same assumptions as Sensor-Based INDI are applied. This yields control law as

$$\boldsymbol{u} = \boldsymbol{u}_0 + \boldsymbol{g}_{\text{mod}}^{-1}(\boldsymbol{x}_0)\left[\boldsymbol{\nu} - \boldsymbol{f}_{\text{mod}}(\boldsymbol{x}_0) - \boldsymbol{g}_{\text{mod}}(\boldsymbol{x}_0)\boldsymbol{u}_0\right]. \tag{8}$$

For this condition, further simplification removes the control increment, $\boldsymbol{u}_0$:

$$\boldsymbol{u} = \boldsymbol{g}_{\text{mod}}^{-1}(\boldsymbol{x}_0)(\boldsymbol{\nu} - \boldsymbol{f}_{\text{mod}}(\boldsymbol{x}_0)). \tag{9}$$

This simplified version of Model-Based INDI is equivalent to the NDI control law. Both the model of the plant dynamics and the control effectiveness matrix appear in the equation. Therefore, the method requires a full system model.

III. Hybrid Incremental Nonlinear Dynamic Inversion

Considering the angular rate control application of INDI, angular rates are regarded to be states and angular accelerations are state derivatives. Control law requires angular accelerations that are not readily available and angular accelerometers are not very common [18]. Aircraft are generally equipped with gyroscopes that measure angular rates. To obtain angular accelerations, angular rates are differentiated. Differentiation of a noisy signal magnifies the amplitude of the noise, which causes the need for additional noise filtering. Sensor dynamics and noise filtering introduce time lags to the measurements. This is seen as one of the main challenges of Sensor-Based INDI [9]. The proposed Hybrid INDI approach aims to alleviate this problem by fusing sensor measurement and system model with a complementary filter.

Hybrid INDI is designed to include characteristics of Model-Based and Sensor-Based INDI. The difference between approaches is the way to obtain the state derivative $\dot{\boldsymbol{x}}_0$. In Hybrid INDI, the signals are merged to complement each other in the frequency domain. Filter residual is referred to as state derivative estimation and denoted by $\hat{\dot{\boldsymbol{x}}}_0$. The estimation by the complementary filter is given by

$$\hat{\dot{\boldsymbol{x}}} = f(\boldsymbol{x}_s, \dot{\boldsymbol{x}}_m) \tag{10}$$

where f represents a complementary function, $\boldsymbol{x}_s$ is the measurement of the state and $\boldsymbol{x}_m$ is the output of the on-board model. Replacing the state derivative in Eq. (6) with the state derivative estimate, yields the Hybrid INDI control law as

$$\boldsymbol{u} = \boldsymbol{u}_0 + \boldsymbol{g}^{-1}(\boldsymbol{x})(\boldsymbol{\nu} - \hat{\dot{\boldsymbol{x}}}_0). \tag{11}$$

Hybrid INDI uses combination of gyroscope measurement, $\boldsymbol{x}_s$ and model output, $\boldsymbol{x}_m$. Gyroscope measurement is different from $\boldsymbol{x}_0$ because of measurement dynamics and noise filtering, and model output is different from $\boldsymbol{x}_0$ because the model is not equivalent to the real system and external disturbances are not reflected by $\boldsymbol{x}_m$.

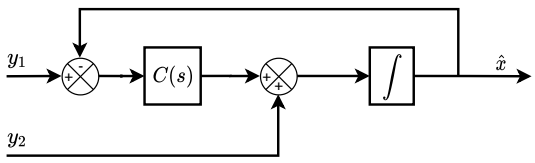

Fig. 1 Block diagram of a classical complementary filter for attitude estimation [25]

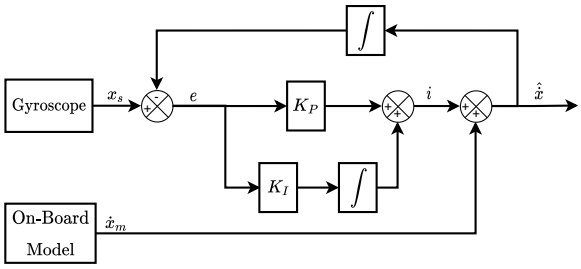

Fig. 2 Block diagram of complementary filter for angular acceleration estimation

A. Complementary Filter for Angular Acceleration Estimation

Traditional complementary filters combine multiple signals to alleviate noise distortions. A signal with low-frequency noise characteristics is high-pass filtered and added to a low-pass filtered signal with high-frequency noise characteristics. Setting the cut-off frequency of filters equal to each other complements the signals and an all-pass estimate is obtained. Such complementary filters are commonly used in the aerospace field for attitude estimation by fusing gyroscope and linear accelerometers [22, 23]. A block diagram of a classical complementary filter is given at Fig. 1 where y_1 is the measurement of the state x and y_2 is the measurement of the state derivative. The filter includes a compansator $C(s)$, that is designed for estimation error dynamics and generally exploits the classical linear control method.

A similar complementary filter is proposed by Jiali and Jihong for the estimation of angular acceleration [24]. It utilizes angular rate measurements by gyroscopes and angular acceleration calculations by a mathematical model. The block diagram of the complementary filter is given in Fig. 2. Notice that the integral block is moved to the feedback signal, since the estimation is for the state derivative instead of the state. The filter is designed as PI compensator where e denotes the error between gyroscope measurement and estimation, and i represents the innovation signal. Consequently, the dynamics of the estimation is given in the Laplace domain as

$$\hat{\dot{\boldsymbol{x}}} = [\boldsymbol{x}_s - \hat{\boldsymbol{x}}\frac{1}{s}][K_p + \frac{K_I}{s}] + \dot{\boldsymbol{x}}_m \tag{12}$$

defining the innovation and error dynamics as,

$$I(s) = E(s)[K_p + \frac{K_I}{s}], \tag{13}$$

$$E(s) = \boldsymbol{x}_s - \frac{1}{s}\hat{\boldsymbol{x}}, \tag{14}$$

the estimation is the sum of the model output and measurement innovation:

$$\hat{\dot{\boldsymbol{x}}} = I(s) + \dot{\boldsymbol{x}}_m. \tag{15}$$

Eq. 12 can be rearranged as well as

$$\hat{\dot{\boldsymbol{x}}} = S(s)\boldsymbol{x}_s + T(s)\dot{\boldsymbol{x}}_m \tag{16}$$

where

$$S(s) = \frac{K_p s + K_I}{s^2 + K_p s + K_I} s; \quad T(s) = \frac{s^2}{s^2 + K_p s + K_I} \tag{17}$$

$S(s)$ and $T(s)$ complement each other such that $\frac{1}{s}S(s) + T(s) = 1$. Bode plots of $T(s)$ and $S(s)/s$ are shown in Fig. 3 and Fig. 4. By the complementary filter, the sensor measurement is low pass filtered and the model output is high pass filtered. The filter contains low-frequency accuracy of the sensor measurement, which includes external disturbances and model mismatches. The filter also contains the high-frequency prediction of the model. The system model responds fast to inputs whereas the noise levels of the resulting estimate are are typically lower, which makes its high-frequency prediction valuable. The model mismatches act as slowly changing biases and due to their low-frequency characteristics, these biases are removed as well. The filter indirectly differentiates measurements and yet removes the high-frequency noise component. Applying the final value theorem shows that the error of estimation approaches to the error of the gyroscope [26]. In this way, the Hybrid approach can largely preserve Sensor-Based INDI's robustness against

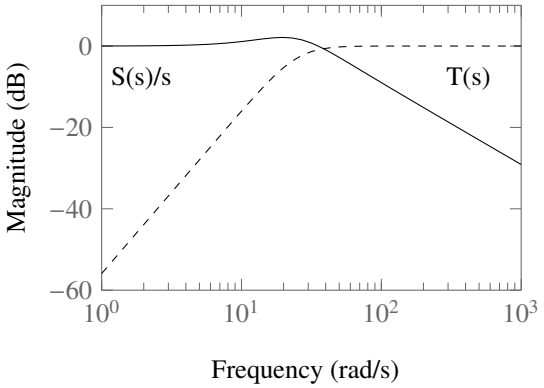

Fig. 3 Bode magnitude plots for complementary filter transfer functions

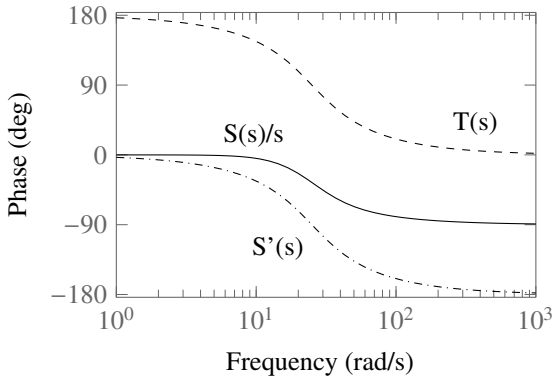

Fig. 4 Bode phase plots for complementary filter transfer functions

uncertainties. Equation 15 shows that without the innovation from the sensor measurement the estimation is only based on the model output and the control method becomes Model-Based INDI.

Crossover frequency and damping coefficient of the filter are set by linear controller gains, $K_I = \omega_n^2$ and $K_p = 2\zeta\omega_n$. The values are selected based on the characteristics of the signals. A lower ω_n filters more of the sensor noise, but the response to external disturbances and model mismatches become slower. The integral gain, K_I, in classical complementary filters are included to compensate gyroscope bias [25]. A constant bias in gyroscope does not affect angular acceleration in INDI applications because of differentiation [19]. The gains set the estimation characteristics and also determine robustness against measurement delays.

B. Nominal Performance Analysis

In this section, the effect of synchronization filter on the nominal performance of Sensor-Based INDI and Hybrid INDI are investigated. For the analysis, a simple system with a state measurement sensor, noise filter dynamics, and actuator dynamics is used. Linearization by INDI and NDI aims to form single integrator dynamics between desired state derivative ν and actual state. A linear kinematic equation;

$$\dot{x} = u \tag{18}$$

is in the form of general nonlinear equation as in Eq. 1 where $f(x) = 0$ and $g(x) = 1$. This equation is selected for analysis purposes since it does not require linearization by INDI and helps to focus on time mismatch analysis. To form a closed loop system, sensor dynamics are added as

$$L'(s) = \frac{1}{t_1 s + 1} e^{-s\tau} \tag{19}$$

where t_1 is time constant which is selected as 0.033 and τ is unknown time delay. The actuator dynamics are given by

$$A(s) = \frac{1}{t_2 s + 1} \tag{20}$$

where t_2 is time constant of the actuator, selected to be 0.05. A noise filter is included in the system which differentiates the state and filters the sensor noise. The noise filter is in the form of

$$H_{\mathrm{F}}(s) = \frac{K_I s}{s^2 + K_p s + K_I} \tag{21}$$

where $K_I = 625$ and $K_P = 35$. The gains for the noise and complementary filter are set to the same values. The block diagrams for the Sensor-Based INDI and Hybrid INDI control architectures are given in Fig. 5.

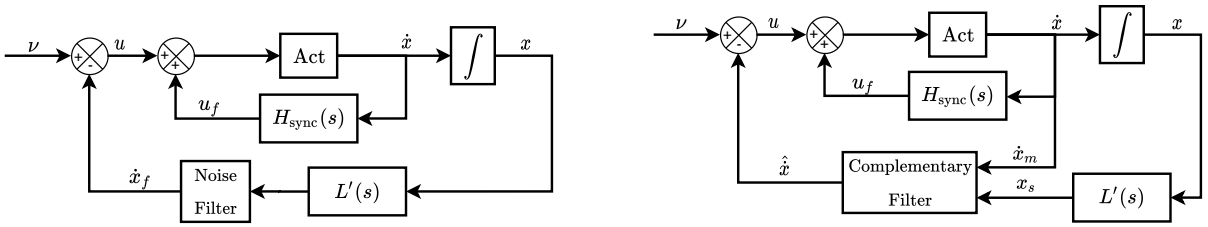

(a) Sensor-Based INDI **(b) Hybrid INDI**

Fig. 5 Block diagrams for the time mismatch robustness analysis

In Section II it is stated that Sensor-Based INDI control law requires a synchronization filter for the control input feedback. The natural choice of the filter for this case comprises of sensor and noise filter dynamics. $L(s) = \frac{1}{t_1 s+1}$ is used in the synchronization because the time delay is assumed to be unknown. Synchronization filter is given by

$$H_{\text{sync}}(s) = L(s)\frac{H_{\text{F}}(s)}{s} \tag{22}$$

In order to show the need for the synchronization filter for Sensor-Based INDI, a nominal case is examined such that there is no unexpected time delay, i.e., $\tau = 0$ and the synchronization filter for both of the approaches are $H_{\text{sync}}(s) = 1$. Figure 6 shows that the response of Sensor-Based INDI is oscillatory with very high magnitudes and the closed loop system is close to become unstable. In Hybrid INDI, when there is a fast changing dynamics, the state derivative information obtained via complementary filter approximates to on-board model calculation. Assuming there is no model mismatches, $\dot{\boldsymbol{x}}_0$ is indeed available. Hence, the synchronization filter in practical application of Hybrid INDI is not as crucial as in Sensor-Based INDI.

Although the performance of Hybrid INDI is sufficiently well without a synchronization filter, the method can benefit from synchronization for a better performance. Following a similar design procedure as in Sensor-Based INDI, control input feedback via the complementary filter yields the ideal synchronization filter for Hybrid INDI as

$$u_f = \frac{S(s)}{s}L(s)u + T(s)u \tag{23}$$

Using this control input feedback makes the closed loop dynamics of Hybrid INDI equivalent to the closed loop dynamics of Sensor-Based INDI with synchronization filter as given in Eq. 22. Hence, the nominal performances of both approaches are identical. The resulting step response is shown in Fig. 7. Along with the significant performance improvement of Sensor-Based INDI, it is shown that overshoot is eliminated and the performance of Hybrid INDI improves in terms of faster settling time.

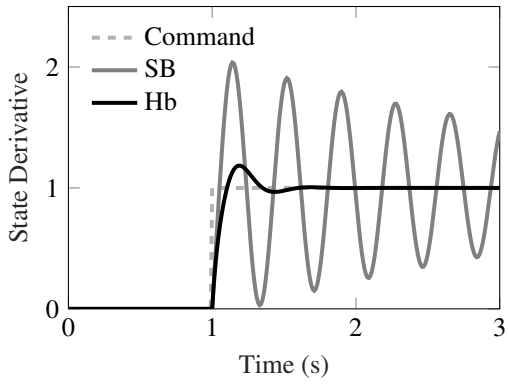

Fig. 6 Nominal performance of Sensor-Based INDI (SB) and Hybrid INDI (Hb) when there is no synchronization filter included. Hybrid INDI performs sufficiently well without synchronization.

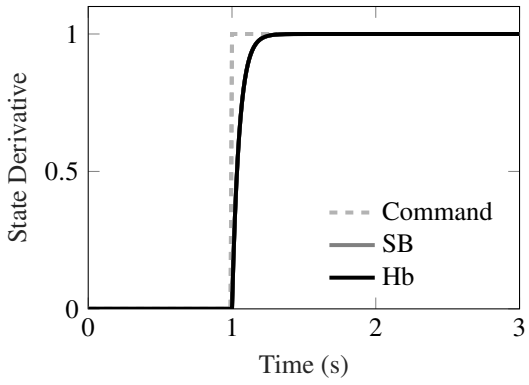

Fig. 7 Nominal performances of Sensor-Based INDI (SB) and Hybrid INDI (Hb) with the synchronization filters included. The performance of both approaches is the same.

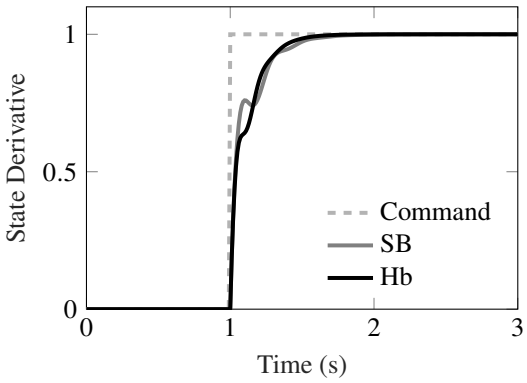

Fig. 8 The nominal performance of the approaches are shown as the synchronization filters of Sensor-Based INDI and Hybrid INDI are modified to be robust against time mismatches. The nominal performance of Sensor-Based INDI degrades more compared to Hybrid INDI.

C. Alternative Synchronization Filter for Hybrid INDI

Past research has demonstrated that INDI is more robust against actuator delays than measurement delays [16]. Including additional delays in actuator measurement is equivalent to synchronization filter with overestimation of state measurement delay. Hence, the claim also means that Sensor-Based INDI does not get affected by overestimation of the measurement delay as much as underestimation. By a modification in the synchronization filter, robust stability levels of Sensor-Based INDI against measurement delays can be improved. A new synchronization filter is given as

$$H'_{\text{sync,SB}}(s) = L(s)\frac{H_{\text{F}}(s)}{s}e^{-s\tau_e} \tag{24}$$

for Sensor-Based INDI, where τ_e is the overestimation of the known time lag to deal with unexpected measurement delays. Similarly, the synchronization filter can be modified for Hybrid INDI as

$$H'_{\text{sync,Hb}}(s) = \frac{S(s)}{s}L(s)e^{-s\tau_e} + T(s) \tag{25}$$

The modification helps the system to have a good performance when the specific unexpected delay is encountered. However, the nominal performance degrades. After setting $\tau_e = 0.07$ and keeping $\tau = 0$, the effect of the alternative synchronization filters are shown in Fig. 8. Both of the approaches compromise their nominal performances to be more robust against time delays, although the nominal performance degradation of Sensor-Based INDI is significantly more than Hybrid INDI.

Instead of selecting τ_e, Hybrid INDI can be made robust against measurement time delays by using the low pass component of the complementary filter in the synchronization filter. A slightly modified version of $S(s)$ as

$$S'(s) = \frac{K_I}{s^2 + K_p s + K_I} \tag{26}$$

can be used for synchronization for Hybrid INDI. Note that, $K_p s$, is removed to be able to have the additional phase delay since that term introduces a lead in the dynamics. Fig. 4 shows that by this modification, there is more phase shift then the amount that complementary filter introduces.

D. Robust Performance Analysis

To show the robustness of Hybrid INDI against measurement delays, a pole migration analysis is performed using the synchronization filter as given in Eq. 26. The pole locations are recorded as the time delay τ is increased up to 0.20 s by 0.02 s increments. The locations of the system poles are shown in Fig. 9a for Sensor-Based INDI. The figure shows that the poles crosses unstable region as the delay increases. This crossing corresponds to 0.18 seconds of delay. By contrast, Hybrid INDI poles remain in the stable region as shown in Fig. 9b. These results are verified by a time-domain simulation. Measurement delay is selected as $\tau = 0.05$ s and the step responses of the systems are plotted in Fig. 9c. The

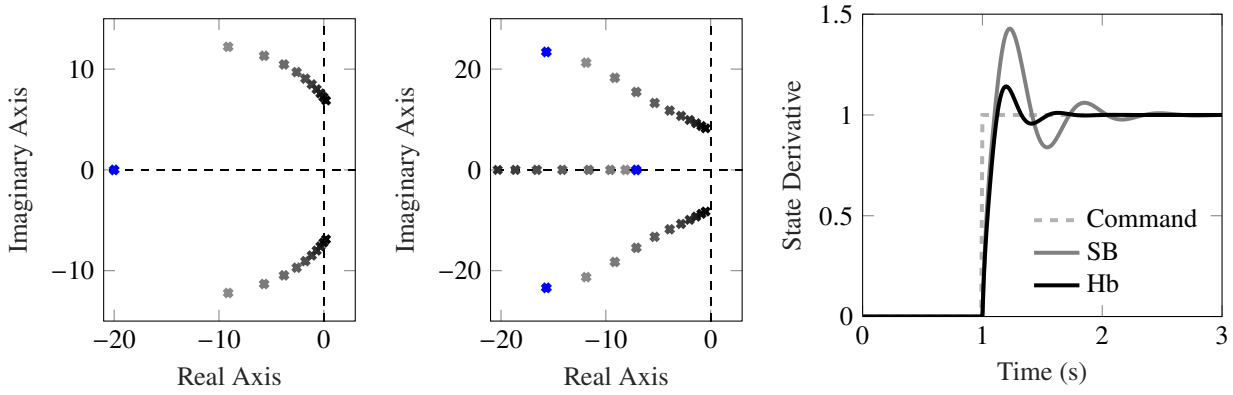

(a) Sensor-Based INDI **(b) Hybrid INDI** **(c) Step response**

Fig. 9 Pole locations in complex plane for various measurement delays (a) Sensor-Based INDI, (b) Hybrid INDI, (c) shows time domain simulation results when measurement delay is 0.07s.

results indicate that underestimation of measurement lag causes significant performance degradation for Sensor-Based INDI. For both systems, performance degrades but Hybrid INDI outperforms Sensor-Based INDI by achieving less overshoot and a faster settling time.

The damping coefficient, ζ, of the filter should be designed based on the desired nominal performance. Increasing damping coefficients slows the step response. Figure 10 shows the effect of damping coefficients on nominal performance. Migration of system poles are shown in Fig. 10a. The complex pair shifts from damping value of 0.18 to 0.55 as ζ increases from 0 to 1. A low ζ causes oscillations and a high value yields a long settling time. Three different step responses are shown in Fig. 10b. According to this analysis, a damping coefficient around 0.5 yields the best performance. However, the pole migration shows that the robustness against measurement delay is affected by ζ as well. A lower damping coefficient causes a faster transition to the unstable region. Therefore, a value of 0.7 is selected.

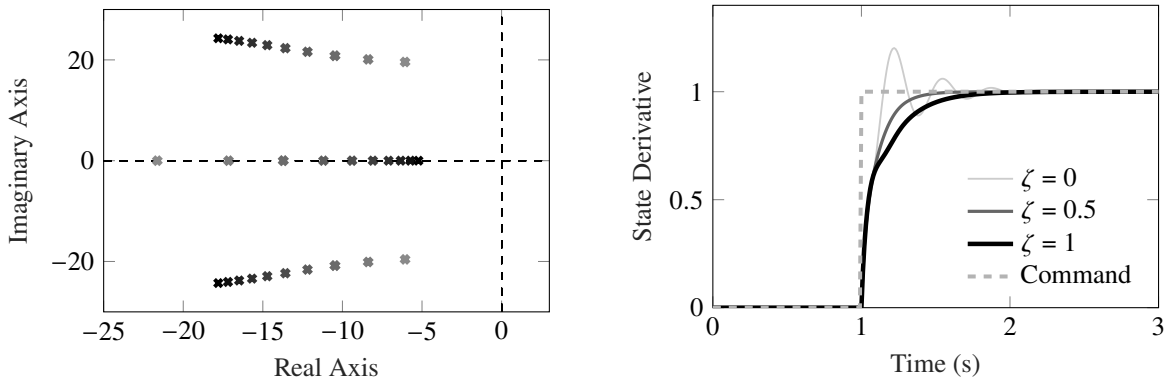

(a) Complex poles moves left of the plane as damping increases **(b) The effect of damping coefficient on step response**

Fig. 10 Effect of damping coefficient of complementary filter on the closed-loop dynamics of Hybrid INDI

IV. Hybrid INDI Flight Control Design for F-16 Aircraft

The objective of this Section is to design an attitude controller for an F-16 aircraft model to robustly track pitch and roll angle commands while regulating the yaw angle. A cascaded control structure is presented based on the time scale separation between angular rates and angular accelerations. The inner loop is designed for tracking desired angular rates, and the outer loop is designed to obtain the desired angular rates to achieve commanded attitude angles.

Table 1 Actuation system characteristics

Actuator	Upper Level Limit	Lower Level Limit	Rate Limits	Time Constant
Throttle (δ_{th})	19000 lbf	1000 lbf	±10000 lbf/s	1 s
Elevator (δ_{e})	25°	-25°	$\pm 60°/s$	0.0495 s
Rudder (δ_{r})	30°	-30°	$\pm 120°/s$	0.0495 s
Aileron (δ_{a})	21.5°	-21.5°	$\pm 80°/s$	0.0495 s

Table 2 Standard Deviations of Measurement Noise

V	$\alpha, \beta, \phi, \theta, \psi$	p, q, r	h
1 m s^{-1}	0.1°	0.01° s^{-1}	5 m

A. Aircraft Model

An open-source F-16 aircraft model is used to test the proposed control method [27–29]. The model is valid up to Mach 0.6 within a constrained flight envelope for angle of attack $-10° \leq \alpha \leq 45°$, sideslip angle $-30° \leq \beta \leq 30°$, velocity 300 ft/s $\leq V \leq$ 900 ft/s and altitude 5000 ft $\leq h \leq$ 40000 ft. The model has three conventional control surfaces: elevator, rudder and aileron to generate pitch, yaw and roll moments. An engine mounted in the rear fuselage provides thrust. Actuators of the aircraft controls are modeled as first-order transfer functions. Characteristics of actuators are presented in Table 1. The actuator dynamics are assumed to be accurately known, which implies that additional sensor dynamics to measure actuator deflections are not included in the simulation.

The model is augmented with sensor models that originate from the GARTEUR High Incidence Research Model (HIRM) [30]. Sensor dynamics to measure body axes attitudes (ϕ, θ, ψ) is

$$L_\theta(s) = \frac{1}{0.00104s^2 + 0.0323s + 1}. \tag{27}$$

Body axes angular rates (p, q, r) are measured by sensors with dynamics of

$$L_\omega(s) = \frac{0.0001903s^2 - 0.005346s + 1}{0.0004942s^2 + 0.03082s + 1}. \tag{28}$$

Air data signals (V_T, α, β, h) are measured by sensors with first-order dynamics,

$$L_a(s) = \frac{1}{0.02s + 1}. \tag{29}$$

In addition, all sensors have additional dynamics that originate from flight control computer's computational delay and analog-to-digital conversion. In addition, air data and attitude sensors are filtered for anti-aliasing. Averaging dynamics are added to angular rate measurements. The details of these additional dynamics are found in [30]. Uncorrelated zero-mean white noise signals are added to the outputs of sensor measurements. The standard deviations of white noise are presented in Table 2 which are based on a previous study with the same aircraft model [31].

The aircraft is modeled symmetric in x-z plane *i.e.* the moment of inertia $J_{xy} = J_{yz} = 0$. The inertia tensor is

$$J = \begin{bmatrix} J_{xx} & 0 & -J_{xz} \\ 0 & J_{yy} & 0 \\ -J_{xz} & 0 & J_{zz} \end{bmatrix}. \tag{30}$$

Total moment vector around body axes $\boldsymbol{M}$ is given by

$$\boldsymbol{M} = J\dot{\boldsymbol{\omega}} + \boldsymbol{\omega} \times J\boldsymbol{\omega}. \tag{31}$$

where angular rates $[p\ q\ r]^T$ are denoted by $\boldsymbol{\omega}$. The moments due to aerodynamics are denoted by L, M and N, they represent rolling, pitching and yawing moments respectively, and given as

$$\boldsymbol{M} = \begin{bmatrix} L \\ M \\ N \end{bmatrix} = \frac{1}{2}\rho V^2 S \begin{bmatrix} b\, C_l \\ \bar{c}\, C_m \\ b\, C_n \end{bmatrix} \tag{32}$$

where b is the wing span, $\hat{c}$ represents the mean aerodynamic cord, ρ is air density, V is airspeed, S is wing surface area, and C_l, C_m, C_n are non-dimensional aerodynamic coefficients. The coefficients are gathered in data tables obtained from wind tunnel tests [32]. The model utilizes coefficient tables given in [29] by linear interpolation. An overview of these values are represented as

$$C_l = C_{l_0}(\alpha,\beta) \;+\; C_{l_p}(\alpha)\frac{pb}{2V} \;+\; C_{l_r}(\alpha)\frac{rb}{2V} \;+\; C_{l_{\delta_a}}(\alpha,\beta)\delta_a \;+\; C_{l_{\delta_r}}(\alpha,\beta)\delta_r \tag{33}$$

$$C_m = C_{m_0}(\alpha,\delta_e) \;+\; C_{m_q}(\alpha)\frac{q\bar{c}}{2V} \;+\; C_z(\alpha,\beta,\delta_e,q)(X_{\mathrm{cgR}} - X_{\mathrm{cg}}) \tag{34}$$

$$C_n = C_{n_0}(\alpha,\beta) \;+\; C_{n_p}(\alpha)\frac{pb}{2V} \;+\; C_{n_r}(\alpha)\frac{rb}{2V} \;+\; C_{n_{\delta_a}}(\alpha,\beta)\delta_a \;+\; C_{n_{\delta_r}}(\alpha,\beta)\delta_r \tag{35}$$

where X_{cgR} represents the reference center of gravity location, which is set at $0.35\bar{c}$. To bring the equations of motion in general nonlinear form as given in Eq. 1, control surface moments should be distinguished from moments due to airframe. The equations of C_l and C_n are control-affine, which makes the distinguishing straightforward; however, C_m is not affine in the control input. To separate contribution of elevator deflection from C_{m_0}, the rate of change of coefficients with respect to δ_e is calculated. Effect of elevator deflection on C_z is assumed to be negligible. The moments are rewritten as

$$\begin{bmatrix} L \\ M \\ N \end{bmatrix} = \frac{1}{2}\rho V^2 S \begin{bmatrix} b\, C_{l_{\delta_a}} & 0 & b\, C_{l_{\delta_r}} \\ 0 & \bar{c}\, C_{m_{\delta_e}} & 0 \\ b\, C_{n_{\delta_a}} & 0 & C_{n_{\delta_r}} \end{bmatrix} \begin{bmatrix} \delta_a \\ \delta_e \\ \delta_r \end{bmatrix} + \frac{1}{2}\rho V^2 S \begin{bmatrix} b\, C_{l_a} \\ \bar{c}\, C_{m_a} \\ b\, C_{n_a} \end{bmatrix} \tag{36}$$

where C_{l_a}, C_{m_a}, C_{n_a} denote aerodynamic coefficients of the airframe excluding the effects of control surfaces. Equation (31) and Eq. (36) are combined to solve for angular acceleration $\dot{\boldsymbol{\omega}}$. This yields

$$\dot{\boldsymbol{\omega}} = J^{-1}\left\{\frac{1}{2}\rho V^2 S \begin{bmatrix} b\, C_{l_a} \\ \bar{c}\, C_{m_a} \\ b\, C_{n_a} \end{bmatrix} - \boldsymbol{\omega} \times J\boldsymbol{\omega}\right\} + J^{-1}\frac{1}{2}\rho V^2 S \begin{bmatrix} b\, C_{l_{\delta_a}} & 0 & b\, C_{l_{\delta_r}} \\ 0 & \bar{c}\, C_{m_{\delta_e}} & 0 \\ b\, C_{n_{\delta_a}} & 0 & C_{n_{\delta_r}} \end{bmatrix} \begin{bmatrix} \delta_a \\ \delta_e \\ \delta_r \end{bmatrix}. \tag{37}$$

B. Angular Rate Control Loop

The angular rate controller forms the inner loop of the control structure. The equation for angular acceleration given in Eq. (37) is in the form of general nonlinear equation as in Eq. (1), which is useful for control design. The control effectors are aileron, elevator and rudder. Engine thrust is kept constant. Control variables, virtual controls, and state derivative estimates are

$$\boldsymbol{u} = \begin{bmatrix} \delta_a \\ \delta_e \\ \delta_r \end{bmatrix}; \quad \boldsymbol{\nu_{\dot{\omega}}} = \begin{bmatrix} \nu_{\dot{p}} \\ \nu_{\dot{q}} \\ \nu_{\dot{r}} \end{bmatrix}; \quad \hat{\dot{\boldsymbol{\omega}}} = \begin{bmatrix} \hat{\dot{p}} \\ \hat{\dot{q}} \\ \hat{\dot{r}} \end{bmatrix}. \tag{38}$$

The control effectiveness matrix is inverted to apply the Hybrid INDI approach as given by Eq. (11), which yields the control law as

$$\begin{bmatrix} \delta_a \\ \delta_e \\ \delta_r \end{bmatrix} = \begin{bmatrix} \delta_{a_0} \\ \delta_{e_0} \\ \delta_{r_0} \end{bmatrix} + \frac{J}{\frac{1}{2}\rho V^2 S} \begin{bmatrix} b\, C_{l_{\delta_a}} & 0 & b\, C_{l_{\delta_r}} \\ 0 & \bar{c}\, C_m & 0 \\ b\, C_{n_{\delta_a}} & 0 & C_{n_{\delta_r}} \end{bmatrix}^{-1} \left\{ \begin{bmatrix} \nu_{\dot{p}} \\ \nu_{\dot{q}} \\ \nu_{\dot{r}} \end{bmatrix} - \begin{bmatrix} \hat{\dot{p}} \\ \hat{\dot{q}} \\ \hat{\dot{r}} \end{bmatrix} \right\}. \tag{39}$$

The virtual input vector $\boldsymbol{\nu_{\dot{\omega}}}$ represents the desired angular acceleration. Its dynamics is based on the error between desired angular rates and measured angular rates. The virtual angular acceleration input is given as

$$\boldsymbol{\nu_{\dot{\omega}}} = \boldsymbol{K_{P_\omega}}(\boldsymbol{\omega_d} - \boldsymbol{\omega_s}) + \boldsymbol{K_{D_\omega}}(\dot{\boldsymbol{\omega}}_{\boldsymbol{d}} - \dot{\boldsymbol{\omega}}_{\boldsymbol{s}}) + \dot{\boldsymbol{\omega}}_{\boldsymbol{d}} \tag{40}$$

where $\boldsymbol{\omega_d}$ is the desired angular rates and they are the output of the outer loop, and $\boldsymbol{\omega_s}$ is measured angular rates. The derivative of desired angular rate and measurement is obtained based on the derivative filter given as

$$H_{\mathrm{d}}(s) = \frac{s}{\frac{1}{30}s + 1}. \tag{41}$$

The linear controller consists of a set of proportional and derivative gains, *i.e.* the PD compensator is designed for the error dynamics, and a feedforward term based on the derivative of the desired angular rates is included. Depending on the required response characteristics, the feedback controller can be adjusted to be PI or PID compensator [16]. The integrator term is omitted in this study, since the optimization results detailed in Section IV.D, yield these values close to be close to zero.

C. Attitude Control Loop

The attitude control loop controls roll, pitch, and yaw angles. According to time scale separation, angular rates are assumed to have reached their desired values very fast compared to the dynamics of the inner loop. Attitude control is based on NDI. The kinematic relation between attitude angles and angular rates are given as

$$\begin{bmatrix} \dot{\phi} \\ \dot{\theta} \\ \dot{\psi} \end{bmatrix} = \begin{bmatrix} 1 & \tan\theta\sin\phi & \tan\theta\cos\phi \\ 0 & \cos\phi & -\sin\phi \\ 0 & \sin\phi/\cos\theta & \cos\phi/\cos\theta \end{bmatrix} \begin{bmatrix} p \\ q \\ r \end{bmatrix}. \tag{42}$$

Applying NDI control law yields

$$\begin{bmatrix} p_d \\ q_d \\ r_d \end{bmatrix} = \begin{bmatrix} 1 & \tan\theta\sin\phi & \tan\theta\cos\phi \\ 0 & \cos\phi & -\sin\phi \\ 0 & \sin\phi/\cos\theta & \cos\phi/\cos\theta \end{bmatrix}^{-1} \begin{bmatrix} \nu_{\dot{\phi}} \\ \nu_{\dot{\theta}} \\ \nu_{\dot{\psi}} \end{bmatrix}. \tag{43}$$

The virtual input $\boldsymbol{\nu_{\dot{\theta}}}$ is used as desired attitude angle derivatives. It is based on the error dynamics between the attitude angle commands and measured attitude angles. The relation is given as

$$\boldsymbol{\nu_{\dot{\theta}}} = \boldsymbol{K_{P_\theta}}(\boldsymbol{\theta_r} - \boldsymbol{\theta_s}) + \dot{\boldsymbol{\theta}}_{\boldsymbol{r}} \tag{44}$$

where $\boldsymbol{\theta_r}$ is the reference attitude angle commands and $\boldsymbol{\theta_s}$ is the measured attitude angles. To define the desired closed loop dynamics and to avoid unachievable control inputs, these commands are pre-filtered. The filter is designed to track commands as fast as the system dynamics allow. First-order lag filter is given as

$$H_{\mathrm{pf}}(s) = \frac{1}{0.25s + 1} \tag{45}$$

Setting a lower bandwidth decreases the response time of the system and a high bandwidth causes actuator to reach its limits easier. Since the system cannot respond any faster when the actuator saturates, the higher bandwidth dynamics becomes redundant.

D. Control System Overview

The overall block diagram of the Hybrid INDI-based control system is given in Fig. 11. The control gains $\boldsymbol{K_{P_\theta}}$, $\boldsymbol{K_{P_\omega}}$ and $\boldsymbol{K_{D_\omega}}$ are three by three diagonal matrices. In order to tune these parameters, an optimization algorithm is used. The objectives of the optimization are minimizing root mean square of tracking error of attitude angles and control effort spend by actuators in a nominal case simulation without any uncertainties. The control effort is based on additional deflection of the actuator at each time step, and it is calculated as

$$\delta_E = \sum_{i=1}^{3}\sum_{k=0}^{N} |\delta_i(k) - \delta_i(k-1)|\, dt \tag{46}$$

where i is used for control surfaces and N is the number of sampled data. RMS of tracking error ϵ is given by

$$\epsilon^2 = \frac{\sum_{l=1}^{3}\sum_{k=0}^{N}\left(\boldsymbol{\theta}_r(k) - \boldsymbol{\theta}(k)\right)^2}{N} \tag{47}$$

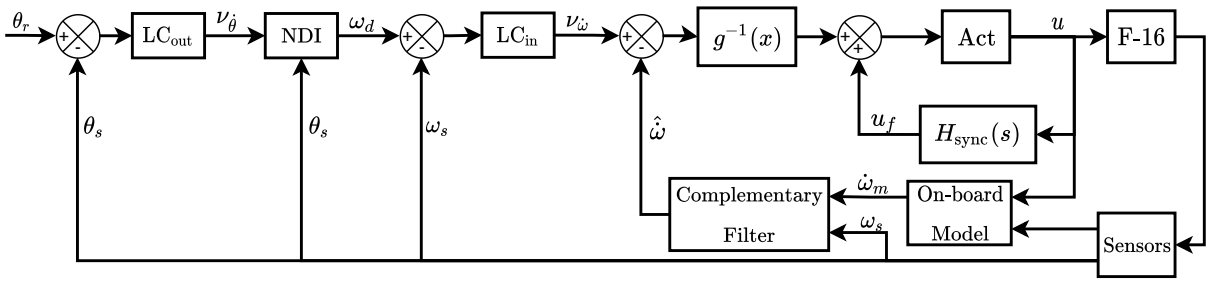

Fig. 11 Overall block diagram of Hybrid INDI

where l denotes control channels of the system. The cost function is simply sum of these two parameters:

$$J = \delta_E + \epsilon \tag{48}$$

By this method, a single metric to evaluate the performance of the control system is obtained. Additional terms can be added based on performance requirements. For instance, a metric to detect oscillations is proposed in [33]. The gains are found by minimizing the cost function and they are given in the Table 3.

Table 3 Linear Control Gains for Sensor-Based and Hybrid INDI-based Control Laws

	K_{P_θ}	K_{P_ω}	K_{D_ω}
Roll	1.17	6.68	0.3
Pitch	1.60	4.28	0
Yaw	1.22	3.73	1

Selection of noise filtering in Sensor-Based INDI applications is challenging since more noise filtering means more time lag and slower response [10]. Similarly, the bandwidth of the complementary filter determines noise alleviation as well as response time and model mismatch cancellation. A balance between these perspectives should be found. In this view, the limits for bandwidth are selected based on the time scale separation. Angular accelerations are faster than the attitude angles. Desired attitude angle characteristics are determined by the prefilter given by Eq. 45. Setting the bandwidth below the prefilter bandwidth naturally slows down the attitude response. Therefore, the lower limit for the bandwidth is set to 4 rad/s. Similarly, angular accelerations to respond faster than the actuators do not affect the performance. Hence, the upper limit is set to the bandwidth of actuators, which is given as 20.2 rad/s in Table 1. Between these values, the balanced value is found at 8 rad/s which is close to geometric average of the limits. Hence, the filter gains that defined in Section III.A, are set as $K_I = 64$ and $K_P = 11.2$.

V. Simulation Results

This section presents the simulation results of the F-16 aircraft model with the control system described in Sec. IV. Sampling frequency is fixed at 100 Hz for all simulations. The operating point is selected at an altitude of 10000 ft with the velocity equal to 500 ft/s, in steady flight. The aircraft is trimmed at this operating point and the resulting values are listed in Table 4. The sensor measurement is differentiated to yield angular acceleration using a second order filter

$$H_{\text{NF}}(s) = \frac{40^2 s}{s^2 + 56s + 40^2} \tag{49}$$

Table 4 Aircraft trim values

δ_{th}	δ_{e}	δ_{a}	δ_{r}	α	V_T	h
2081 lbf	−2.25°	0	0	3.60°	500 ft/s	10000 ft

which filters sensor noise as well. In addition, the alternative synchronization filter dynamics as given in Section III.C is used for the Hybrid INDI design, which corresponds to the same structure as the noise filter given above without the additional derivative term and using the K_I and K_P coefficients stated in Section IV.D.

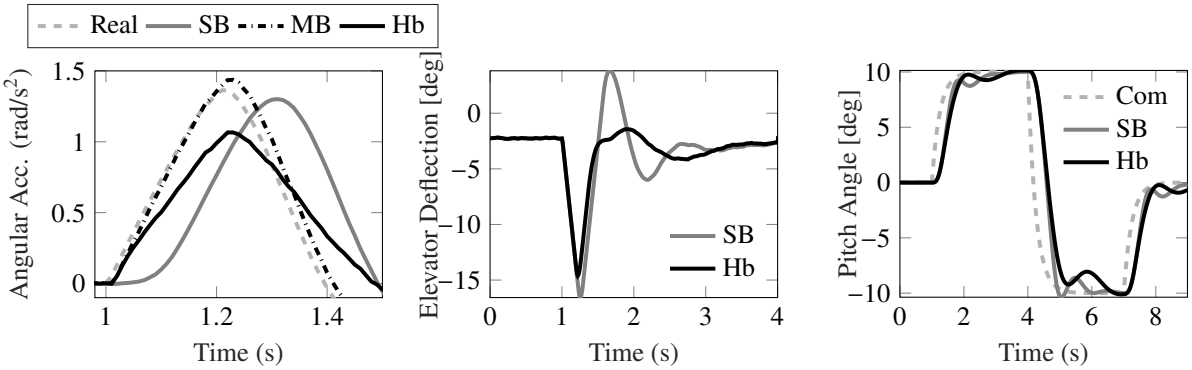

(a) Pitch accelerations obtained by different methods

(b) Elevator deflection

(c) Pitch angle tracking performance

Fig. 12 Response to pitch angle command in nominal conditions sensor and noise filter dynamics are included

To show the differences between the INDI approaches, nominal performance is investigated first. The aircraft is commanded with pitch angle doublet. Pitch accelerations, tracking performance, and elevator deflection are shown in Fig. 12 focusing on different time ranges. Figure 12a shows actual angular acceleration, model output, complementary filter output, and sensor-based acceleration calculation and focuses on the time of initial command. The on-board model matches with the actual aircraft dynamics since no uncertainty is introduced. A difference between the model output and the actual value is caused by time lag of the control inputs to the model. The model also uses the aircraft measurements without any noise filtering. Therefore, angular acceleration measurement lags behind the model output. In addition, aerodynamic moments due to system states do not match with the actual value due to the noisy measurements. Sensor-based angular acceleration is the shifted version of actual value, and shows a good match except for the time lag. The hybrid angular acceleration increases with the model output that increases without any time delay. Then, it starts to converge to the acceleration value from the sensor measurement. Using Hybrid INDI makes the system to respond earlier than the measured states.

Figure 12b compares elevator deflections of Hybrid INDI and Sensor-Based INDI. Around $t = 1.2$ s elevator deflection reverses since the angular rate reaches its desired value. Hybrid INDI experiences this change at a lower magnitude due to the lower bandwidth of the selected complementary filter compared to the noise filter of the Sensor-Based INDI design. Figure 12c shows the time histories of both INDI approaches when subjected to a pitch doublet command. Both responses show similar characteristics such that after one oscillation they settle down. The settling time of Hybrid INDI is slightly higher, causing the RMS error to increase. The performance criteria were set to be the sum of RMS error and control effort. The cost value of both approaches similar in nominal conditions.

Two additional simulations are performed to investigate disturbance rejection and system robustness against aerodynamic uncertainty. The simulation results of disturbance rejection performance of the methods are shown in Fig. 13. In order to simulate a constant wind, a step input is introduced by increasing angle of attack value of the system at time is equal to 1 second. All approaches initially respond to the disturbance similarly. After a short time, Sensor-Based and Hybrid INDI remove the effect of disturbance by setting the angle of attack to its steady-state value. Although, the rejection characteristics are different the settling times of the methods are close to each other. In contrast, Model-Based INDI cannot remove the disturbance and the angle of the attack remains about 0.4° above the trim value since $\boldsymbol{f}_{\text{mod}}$ does not match with real aircraft dynamics and the difference between them acts as bias given to the control law.

In terms of robustness against aerodynamic uncertainty, Hybrid INDI is successful as seen in Fig. 14. A step input is commanded in the pitch channel and the airframe stability derivative coefficients are increased by 50%. The observed time histories of Sensor-Based INDI and Hybrid INDI do not deviate much from their nominal performances, whereas the performance of Model-Based INDI significantly degrades. In particular, the Model-Based INDI design results in a large overshoot, oscillations,and a steady-state tracking error.

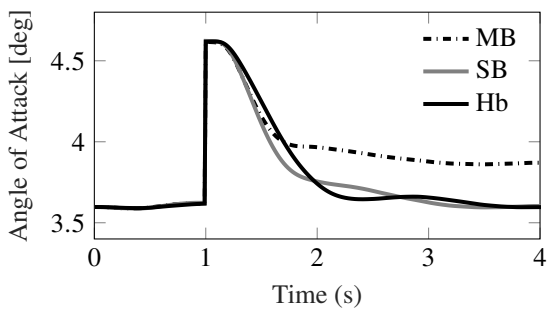

Fig. 13 The responses different INDI approaches in existence of step disturbance as wind gust. Model-Based INDI is not as successful as other approaches, on rejecting the disturbance.

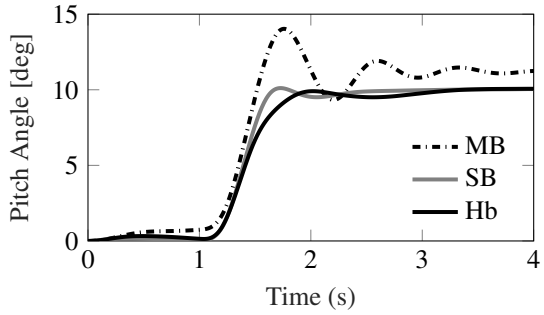

Fig. 14 Stability derivative aerodynamic coefficients are increased by 50% to simulate an uncertainty. Model-Based INDI shows oscillatory behaviour and cannot eliminate steady state error.

To test the robustness of the Hybrid INDI design against measurement delays, a transport delay of 0.05 seconds is introduced in the angular rate measurement in addition to the aerodynamic model offsets. A doublet input is given in pitch and roll, as shown in Fig. 15. The results show that Hybrid INDI is robust against measurement delays, with little deviation from the nominal performance. By contrast, oscillations occur with Sensor-Based INDI. Moreover, it appears that lateral modes are more vulnerable to time delays. For instance, the roll angle oscillates with a magnitude up to 4° although the pitch plane is excited. Additional simulations with increasing time delays show that SB-INDI becomes unstable when the transport delay equals 0.07 seconds, whereas Hybrid INDI stays in the stable region up to 0.13 seconds.

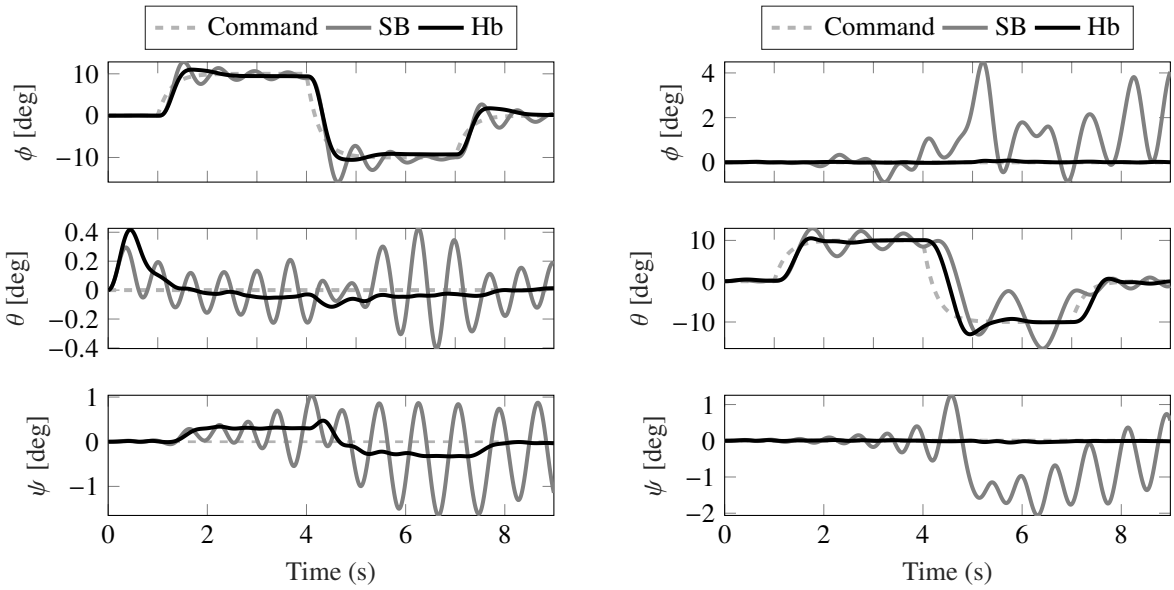

(a) Roll doublet input

(b) Pitch doublet input

Fig. 15 Tracking performances in existence of measurement delays and aerodynamic uncertainties

VI. Conclusions and Recommendations

In this paper, a new form of INDI is proposed that modifies the linearization loop via a complementary filter. The filter generates an angular acceleration estimation based on sensor measurement and on-board model output. Consequently, the resulting Hybrid INDI formulation includes characteristics of both Model-Based INDI and Sensor-Based INDI

strategies. The key feature lies in the alleviation of drawbacks caused by sensor measurement delays by obtaining state derivative information from an on-board model with reduced levels of delay. Hybrid INDI persists to be robust against model mismatches and external disturbances by utilizing low frequency characteristics of measurements.

The effectiveness of the Hybrid INDI has been demonstrated by two types of simulation analysis. The initial analysis considers a simple system and only the linearization loop of INDI is investigated. This analysis compares Sensor-Based INDI and Hybrid INDI in terms of tracking performance in nominal conditions and in the existence of measurement delays. Consequently, it is shown that Hybrid INDI yields less overshoot and faster settling time when the measurement delays are underestimated. Different synchronization filtering options are examined and it is shown that Hybrid INDI performs sufficiently well even without a synchronization filter which is thanks to transient state derivative feedback via the on-board model. In order to further increase the robustness of the method, an alternative synchronization filter is given as a modified transfer function of the complementary filter.

The design procedures are set by analysing a simple dynamical system. Simulation results show the robustness of the method against measurement delays and its ability to maintain the main benefits of the sensor-based nature of INDI. In addition, Hybrid INDI with the proposed alternative synchronization filter loses less tracking performance under nominal conditions compared to Sensor-Based INDI. Simulation scenarios with uncertainties in aerodynamic stability coefficients indicate that the on-board model of Hybrid INDI does not have to be very accurate for the control system to be robust against model mismatches. This finding is underscored by the successful rejection of gust disturbance. Finally, the introduction of measurement delays causes Hybrid INDI not to significantly deviate from its nominal performance levels, whereas the performance of Sensor-Based INDI becomes undesirable due to oscillations in the commanded channel as well as other channels.

In future research, different hybridization or estimation techniques could be used for Hybrid INDI. One possible modification that is worth investigating is to use angular accelerometers instead of gyroscopes. In this study, an angular acceleration estimation method is used for Hybrid INDI since this method has advantages such as being simple and easily adaptable to system requirements. The use of accelerometers can be implemented with a minor change in the complementary filter. Additionally, future studies may consider Kalman filtering as a possible method, which exploits both measurement and model simultaneously.

Another form of Hybrid INDI was proposed in a recent study to solve the problem of abrupt roll motion after store launching on one side of wing in a fighter aircraft [34]. The study shows that Hybrid INDI is successful at alleviating the transient response of the aircraft and decreasing the workload of the pilot. This application of Hybrid INDI indicates that future studies can focus on problems due to sudden changes of the system dynamics. For example, delivery drones are designed to have symmetrical affect on the drone when they remove their loads. Hybrid INDI can increase design flexibility and their capacity since the method can handle the disturbance affect due to unsymmetrical unloading and its reaction effect on the drone itself.

Lastly, future studies can explore Hybrid INDI along with FDI algorithms and fault scenarios. The method appears to be well-suited for fault-tolerant approaches. Switching Hybrid INDI to its components is a trivial procedure such that ignoring on-board model input yields Sensor-Based INDI and removing sensor innovation from state derivative feedback results in Model-Based INDI. This property can be investigated in the future where an FDI algorithm decides which of the two is responsible for the faulty signal.

References

[1] Adams, R. J., and Banda, S. S., "Integrated approach to flight control design using dynamic inversion and μ-synthesis," *American Control Conference*, Vol. 1, No. 2, 1993, pp. 1385–1389. https://doi.org/10.23919/acc.1993.4793098.

[2] Enns, D., Bugajski, D., Hendrick, R., and Stein, G., "Dynamic inversion: An evolving methodology for flight control design," *International Journal of Control*, Vol. 59, No. 1, 1994, pp. 71–91. https://doi.org/10.1080/00207179408923070.

[3] McFarland, M. B., and D'Souza, C. N., "Missile flight control with dynamic inversion and structured singular value synthesis," *Guidance, Navigation, and Control Conference, 1994*, 1994, pp. 544–550. https://doi.org/10.2514/6.1994-3604.

[4] Smith, P., "A simplified approach to nonlinear dynamic inversion based flight control," *23rd Atmospheric Flight Mechanics Conference*, Boston, MA, USA, 1998. https://doi.org/10.2514/6.1998-4461, AIAA-1998-4461.

[5] Smith, P., and Berry, A., "Flight test experience of a non-linear dynamic inversion control law on the VAAC Harrier," *Atmospheric Flight Mechanics Conference*, Denver, CO, USA, 2000. https://doi.org/10.2514/6.2000-3914, AIAA-2000-3914.

[6] Grondman, F., Looye, G., Kuchar, R. O., Chu, Q. P., and Van Kampen, E., "Design and Flight Testing of Incremental Nonlinear Dynamic Inversion-based Control Laws for a Passenger Aircraft," *2018 AIAA Guidance, Navigation, and Control Conference*, Kissimmee, FL, USA, 2018. https://doi.org/10.2514/6.2018-0385, AIAA-2018-0385.

[7] Keijzer, T., Looye, G., Chu, Q. P., and Van Kampen, E., "Design and Flight Testing of Incremental Backstepping based Control Laws with Angular Accelerometer Feedback," *AIAA Scitech 2019 Forum*, San Diego, CA, USA, 2019. https://doi.org/10.2514/6.2019-0129, AIAA-2019-0129.

[8] Pollack, T., Looye, G., and van der Linden, F., "Design and flight testing of flight control laws integrating incremental nonlinear dynamic inversion and servo current control," *AIAA Scitech 2019 Forum*, San Diego, CA, USA, 2019. https://doi.org/10.2514/6.2019-0130, AIAA-2019-0130.

[9] Smeur, E. J., Chu, Q. P., and De Croon, G. C., "Adaptive incremental nonlinear dynamic inversion for attitude control of micro air vehicles," *Journal of Guidance, Control, and Dynamics*, Vol. 39, No. 3, 2016, pp. 450–461. https://doi.org/10.2514/1.G001490.

[10] Smeur, E. J., Bronz, M., and de Croon, G. C., "Incremental Control and Guidance of Hybrid Aircraft Applied to a Tailsitter Unmanned Air Vehicle," *Journal of Guidance, Control, and Dynamics*, Vol. 43, No. 2, 2020, pp. 274–287. https://doi.org/10.2514/1.g004520.

[11] Lu, P., van Kampen, E., de Visser, C., and Chu, Q. P., "Aircraft fault-tolerant trajectory control using Incremental Nonlinear Dynamic Inversion," *Control Engineering Practice*, Vol. 57, 2016, pp. 126–141. URL http://dx.doi.org/10.1016/j.conengprac.2016.09.010.

[12] Sun, S., Sijbers, L., Wang, X., and De Visser, C., "High-Speed Flight of Quadrotor Despite Loss of Single Rotor," *IEEE Robotics and Automation Letters*, Vol. 3, No. 4, 2018, pp. 3201–3207. https://doi.org/10.1109/LRA.2018.2851028.

[13] Sun, S., Wang, X., Chu, Q. P., and de Visser, C., "Incremental Nonlinear Fault-Tolerant Control of a Quadrotor with Complete Loss of Two Opposing Rotors," *arXiv preprint*, 2020. URL http://arxiv.org/abs/2002.07837.

[14] Simplício, P., Pavel, M. D., van Kampen, E., and Chu, Q. P., "An acceleration measurements-based approach for helicopter nonlinear flight control using incremental nonlinear dynamic inversion," *Control Engineering Practice*, Vol. 21, No. 8, 2013, pp. 1065–1077.

[15] Acquatella, P. B., Falkena, W., van Kampen, E., and Chu, Q. P., "Robust nonlinear spacecraft attitude control using incremental nonlinear dynamic inversion," *AIAA Guidance, Navigation, and Control Conference*, Minneapolis, MN, USA, 2012. https://doi.org/10.2514/6.2012-4623, AIAA-2012-4623.

[16] van't Veld, R. C., van Kampen, E., and Chu, Q. P., "Stability and robustness analysis and improvements for incremental nonlinear dynamic inversion control," *AIAA Guidance, Navigation, and Control Conference, 2018*, Kissimmee, FL, USA, 2018. https://doi.org/10.2514/6.2018-1127, AIAA-2018-1127.

[17] Cakiroglu, C., van Kampen, E., and Chu, Q. P., "Robust incremental nonlinear dynamic inversion control using angular accelerometer feedback," *AIAA Guidance, Navigation, and Control Conference, 2018*, 2018. https://doi.org/10.2514/6.2018-1128, AIAA-2018-1128.

[18] Sieberling, S., Chu, Q. P., and Mulder, J. A., "Robust flight control using incremental nonlinear dynamic inversion and angular acceleration prediction," *Journal of Guidance, Control, and Dynamics*, Vol. 33, No. 6, 2010, pp. 1732–1742. https://doi.org/10.2514/1.49978.

[19] Smeur, E. J., de Croon, G. C., and Chu, Q. P., "Cascaded incremental nonlinear dynamic inversion for MAV disturbance rejection," *Control Engineering Practice*, Vol. 73, No. November 2017, 2018, pp. 79–90. https://doi.org/10.1016/j.conengprac.2018.01.003.

[20] Pavel, M. D., Shanthakumaran, P., Chu, Q. P., Stroosma, O., Wolfe, M., and Cazemier, H., "Incremental Nonlinear Dynamic Inversion for the Apache AH-64 Helicopter Control," *Journal of the American Helicopter Society*, Vol. 65, No. 2, 2020, pp. 1–16. https://doi.org/10.4050/JAHS.65.022006.

[21] Wang, X., van Kampen, E., Chu, Q. P., and Lu, P., "Stability Analysis for Incremental Nonlinear Dynamic Inversion Control," *Journal of Guidance, Control, and Dynamics*, Vol. 42, No. 5, 2019, pp. 1116–1129. https://doi.org/10.2514/1.G003791, URL https://arc.aiaa.org/doi/10.2514/1.G003791.

[22] Euston, M., Coote, P., Mahony, R., Kim, J., and Hamel, T., "A complementary filter for attitude estimation of a fixed-wing UAV," *IEEE/RSJ International Conference on Intelligent Robots and Systems, IROS*, IEEE, 2008, pp. 340–345. https://doi.org/10.1109/IROS.2008.4650766.

[23] Wu, J., Zhou, Z., Chen, J., Fourati, H., and Li, R., "Fast Complementary Filter for Attitude Estimation Using Low-Cost MARG Sensors," *IEEE Sensors Journal*, Vol. 16, No. 18, 2016, pp. 6997–7007. https://doi.org/10.1109/JSEN.2016.2589660.

[24] Jiali, Y., and Jihong, Z., "An angular acceleration estimation method based on the complementary filter theory," *IEEE Instrumentation and Measurement Technology Conference*, Vol. 2016-July, 2016, pp. 1–6.

[25] Mahony, R., Hamel, T., and Pflimlin, J.-M., "Nonlinear Complementary Filters on the Special Orthogonal Group," *IEEE Transactions on Automatic Control*, Vol. 53, No. 5, 2008, pp. 1203–1219. https://doi.org/10.1080/00207179.2012.693951.

[26] Yoo, T. S., Hong, S. K., Yoon, H. M., and Park, S., "Gain-scheduled complementary filter design for a MEMS based attitude and heading reference system," *Sensors*, Vol. 11, No. 4, 2011, pp. 3816–3830. https://doi.org/10.3390/s110403816.

[27] Nguyen, L. T., Ogburn, M. E., Gilbert, W. P., Kibler, K. S., Brown, P. W., and Deal, P. L., "Simulator study of stall/post-stall characteristics of a fighter airplane with relaxed longitudinal static stability," Tech. rep., NASA, 1979.

[28] Russell, R. S., "Non-linear F-16 Simulation using Simulink and MATLAB," Tech. rep., University of Minnesota, 2003.

[29] Stevens, B., Lewis, F., and Johnson, E., *Aircraft Control and Simulation: Dynamics, Controls Design, and Autonomous Systems*, Wiley, 2015.

[30] Muir, E., "The GARTEUR High Incidence Research Model (HIRM) benchmark problem," *Guidance, Navigation, and Control Conference and Exhibit*, American Institute of Aeronautics and Astronautics, Boston, MA, USA, 1998. https://doi.org/10.2514/6.1998-4243, AIAA-1998-4243.

[31] van Gils, P., van Kampen, E., de Visser, C. C., and Chu, Q. P., "Adaptive incremental backstepping flight control for a high-performance aircraft with uncertainties," *AIAA Guidance, Navigation, and Control Conference*, San Diego, CA, USA, 2016. https://doi.org/10.2514/6.2016-1380, AIAA-2016-1380.

[32] Nguyen, L., Ogburn, M., Gilbert, W., Kibler, K., Brown, P., and Deal, P., "Simulator Study of Stall/Post-Stall Characteristics of a Fighter Airplane With Relaxed Longitudinal Static Stability," Tech. rep., National Aeronautics and Space Administration, Langley Research Center, Hampton, Virginia, 1979.

[33] Mooij, E., "Robust Control of a Conventional Aeroelastic Launch Vehicle," *AIAA Scitech 2020 Forum*, Orlando, FL, USA, 2020. https://doi.org/10.2514/6.2020-1103, AIAA-2020-1103.

[34] Kim, C.-S., Ji, C.-H., Koh, G.-O., and Kim, B. S., "Stability Margin and Structural Coupling Analysis of a Hybrid INDI Control for the Fighter Aircraft," *International Journal of Aeronautical and Space Sciences*, Vol. 22, No. 5, 2021, pp. 1154–1169.